# Mast cells promote pathology and susceptibility in tuberculosis

Ananya Gupta[1,2], Vibha Taneja[1], Javier Rangel Moreno[3], Abhimanyu[1], Mushtaq Ahmed[1], Nilofer Naqvi[1], Kuldeep S. Chauhan[1], Daniela Trejo-Ponce de León[5,6], Gustavo Ramírez-Martínez[6], Luis Jiménez-Alvarez[6], Cesar Luna-Rivero[6], Joaquin Zuniga[5,6], Deepak Kaushal[6], Shabaana A. Khader[1,2#]

Affiliations:

[1] The University of Chicago, Department of Microbiology, 920 East 58th Street, CLSC 1117, Chicago, IL 60637.

[2] Department of Molecular Microbiology, Washington University in St. Louis, St. Louis, MO 63110, USA

[3] Division of Allergy, Immunology and Rheumatology, Department of Medicine, University of Rochester Medical Center, Rochester, NY, USA

[5] Technologico de Monterrey, Escuela de Medicina y Ciencias de la Salud, Mexico City, Mexico

[6] Laboratory of Immunobiology and Genetics and Department of Pathology, Instituto Nacional de Enfermedades Respiratorias Ismael Cosio Villegas, Mexico

[7] Texas Biomedical Research Institute, San Antonio, Texas 78245-0549, USA.

[#] Correspondence:

Shabaana A. Khader, The University of Chicago, Department of Microbiology, 920 East 58th Street, CLSC 1117, Chicago, IL 60637, Phone: (773)-702-2601. Email-khader@uchicago.edu

**Abstract**

Tuberculosis (TB), caused by the bacterium *Mycobacterium tuberculosis* (*Mtb*), infects approximately one-fourth of the world's population. While most infected individuals are asymptomatic, latent TB infection (LTBI) can progress to cause pulmonary TB (PTB). We recently reported an increased accumulation of mast cells (MCs) in lungs of macaques with PTB, compared with LTBI in macaques. MCs respond in vitro to *Mtb* exposure via degranulation and by inducing proinflammatory cytokines. In the current study, we show the dominant production of chymase by MCs in granulomas of humans and macaques with PTB. Using scRNA seq analysis, we show that MCs found in LTBI and healthy lungs in macaques are enriched in genes involved in tumor necrosis factor alpha, cholesterol and transforming growth factor beta signaling. In contrast, MCs clusters found in PTB express transcriptional signatures associated with interferon gamma, oxidative phosphorylation, and MYC signaling. Additionally, MC deficiency in the mouse model showed improved control of *Mtb* infection that coincided with reduced accumulation of lung myeloid cells and diminished inflammation at chronic stages. Thus, these collective results provide novel evidence for the pathological contribution of MCs during *Mtb* infection and may represent a novel target for host directive therapy for TB.

**Keywords:** Mast cells, Tuberculosis, lung, innate cell, inflammation.

44 **Introduction.** Tuberculosis (TB) remains a significant global health issue, with approximately
45 one-quarter of the world's population harboring *Mycobacterium tuberculosis* (*Mtb*) causing
46 around 1.5 million deaths each year (WHO, 2023). The disease often starts as a latent TB
47 infection (LTBI), in which the bacteria remain dormant and cause no symptoms. However,
48 LTBI can progress to active pulmonary TB (PTB), characterized by severe respiratory
49 symptoms and high transmission potential. The immune mechanisms that allow progression
50 from latent to PTB are not fully defined. Thus, understanding the immune factors that drive
51 progression toward PTB will allow the development of novel therapeutics for TB control.
52 Towards this overall goal, we recently showed that the lung single-cell transcriptional immune
53 landscape during LTBI and PTB in macaques infected with *Mtb* was distinct. For example,
54 PTB was characterized by the significant accumulation of Type I IFN expressing-plasmacytoid
55 DCs (pDCs), IFN-responsive macrophages as well as activated T cells to the lungs, (Esaulova
56 *et al*., 2021). Additionally, mast cells (MCs) were increased in the lungs of macaques with PTB
57 (Esaulova *et al*., 2021). In sharp contrast, LTBI was characterized by increased presence of
58 cytotoxic NK cells but lack of recruitment of MCs in the lungs (Esaulova *et al*., 2021).
59 MCs are found in the lung where they influence inflammatory responses (Naqvi *et al*., 2021).
60 MCs have been shown to respond *in vitro* to *Mtb* exposure via surface receptors such as CD48
61 (Munoz *et al*., 2003). They also react to *Mtb* exposure or mycobacterial lipids by undergoing
62 degranulation of prestored granules such as histamine and β-hexosaminidase, and inducing
63 secretion of proinflammatory cytokines such as IL-6 and TNF-α (Munoz *et al.,* 2003).
64 Degranulation of MCs following intratracheal infection with a high dose of *Mtb* resulted in
65 limiting inflammation and proinflammatory cytokines such as IL-1β and TNF-α (Carlos *et al*.,
66 2007). MCs produce and release either chymase or tryptase (Bian *et al*., 2021) which are both
67 proteases that are stored in the cell's secretory granules. Recent studies with lung biopsies of
68 TB patients showed an enrichment of MCs expressing IL-17 at inflammatory sites. In contrast,

69 chymase rich MCs ($MC_C$s) producing TGF-β were detected in proximity to mature granulomas
70 in lung biopsies from PTB (Garcia-Rodriguez *et al*., 2021). Furthermore, while healthy lung
71 predominantly has tryptase-expressing mast cells ($MC_T$s), both chymase and dual mast cells
72 co-expressing chymase and tryptase ($MC_C$s and $MC_{TC}$s) accumulate in the infected lung of
73 patients with PTB (Garcia-Rodriguez *et al*., 2021). Thus, while previous studies have shown
74 that MCs respond to *Mtb* exposure and accumulate in macaque and human lungs during PTB,
75 it is not completely known if MCs functionally mediate protective or pathological outcomes in
76 the context of TB infection.
77 In the current study, we show that the distribution and localization of MCs in PTB in humans
78 and macaques is associated with chymase production. Using scRNA seq analysis, we show that
79 MCs found in LTBI and healthy lungs in macaques, are transcriptionally distinct than PTB
80 lungs showing enrichment of tumor necrosis factor alpha, cholesterol and transforming growth
81 factor beta signaling, while MCs found in PTB express increased levels of signatures associated
82 with interferon gamma, oxidative phosphorylation, and MYC signaling. Additionally, mice
83 deficient in MCs, showed improved control of *Mtb* infection and reduced lung inflammation,
84 providing novel evidence that chymase positive MCs contribute to immune pathology and
85 reduced *Mtb* control, suggesting a pathological role for MCs during *Mtb* infection.
86
87 **Materials and methods**
88 **Study subjects**
89 All human lung biopsy samples were obtained from the Tuberculosis Outpatient Clinic and the
90 Department of Pathology at the National Institute of Respiratory Diseases (INER) in Mexico
91 City, before *M. tuberculosis* treatment with informed consent, and with the approved protocol
92 by the INER IRB for their use (project numbers B04-15 and B09-23). Also, lung samples from

93 healthy controls (HC) non-TB individuals were obtained from the tissue repository of the
94 Department of Pathology from INER. No compensation was provided to the patients.
95 Non-human primate procedures were approved by the Institutional Animal Care and Use
96 Committee of Tulane National Primate Research Center and were performed in accordance
97 with National Institutes of Health (NIH) guidelines. Male and female Indian rhesus macaques,
98 verified to be free of *Mtb* infection by tuberculin skin test, were obtained from the Tulane
99 National Primate Research Center. The animals were housed in an ABSL3 facility.
100 C57Bl/6 and B6.Cg-KitW-sh/HNihrJaeBsmJ (Strain #:030764) alias $CgKitW^{sh}$ mice were
101 procured from Jackson Laboratory (Bar Harbor, ME) and bred at Washington University in St.
102 Louis. Six to eight weeks female and male mice were used in the experiments. All mice were
103 maintained and used in accordance with the approved Institutional Animal Care and Use
104 Committee (IACUC) guidelines at Washington University in St. Louis.
105
106 **Aerosol Infection**
107 *Mtb* strain HN878 was cultured in Proskauer Beck medium containing 0.05% Tween 80 until
108 reaching mid-log phase and frozen in 1 ml aliquots at -80°C until used. Mice were aerosol
109 infected with ~100 colony forming units (CFU), as described previously (Khader *et al*., 2007).
110 Macaques were assigned to three groups: (1) uninfected control, (2) macaques with LTBI were
111 exposed to a low dose (~10 CFU), and (3) macaques with PTB were exposed to a high dose
112 (~100 CFU) of *Mtb* CDC1551 via the aerosol route using a custom head-only dynamic
113 inhalation system housed within a class III biological safety cabinet as previously described
114 (Esaulova *et al*., 2021). The animals were periodically monitored for detecting alterations in
115 their physiological parameters and to monitor disease symptoms.
116
117 **Bacterial burden and cytokine Analysis**

118 Bacterial burden was assessed using serial 10-fold dilutions of lung or spleen homogenates and
119 plated on 7H11 agar solid medium supplemented with OADC (oleic acid, bovine albumin,
120 dextrose, and catalase). Colonies were counted after 2-3 weeks of incubation.
121 Cytokine/chemokine expression was analyzed in lung homogenates from infected mice via
122 Luminex (Millipore-Sigma) or ELISA (R&D) as per the manufacturer's protocol.
123
124 **Generation of single-cell suspensions from tissues and flow cytometry staining**
125 Lung single-cell suspensions from *Mtb*-infected mice were prepared as previously described
126 (Gopal *et al*., 2013). Briefly, mice were euthanized with $CO_2$. The right lower lobe was isolated
127 and perfused with heparin in saline. Lungs were minced and incubated with
128 collagenase/DNAse for 30 minutes at 37°C. Lung tissue was pushed through a 70µm nylon
129 screen to obtain a single cell suspension. Following lysis of erythrocytes, the cells were washed
130 and resuspended in cDMEM (DMEM high glucose + 10% fetal bovine serum + 1%
131 Penicillin/Streptomycin) for flow cytometry staining. For flow cytometric analysis, cells were
132 either stained immediately, or stimulated with phorbol myristate acetate (PMA-50ng/ml;
133 Sigma Aldrich) and ionomycin (750 ng/ml; Sigma Aldrich) in the presence of Golgistop (BD
134 Pharmingen).
135 The following fluorochrome conjugated antibodies were used for myeloid cell surface staining
136 CD11b APC (clone M1 / 70), CD11c PeCy7 (clone HL3, BD Biosciences) GR-1 PerCP-Cy5.5
137 (Clone RB6-8C5, BD Pharmingen) and MHC class II FITC (Clone M5/114.15.2, Tonbo
138 Biosciences), Anti-Mo CD117 (cKit) super bright 780 (eBiosciences; clone 2BB), FcεR1 PE
139 (eBiosciences; clone MAR-1). Myeloid cells: alveolar macrophages were gated on
140 $CD11c^{+}CD11b^{-}$, neutrophils were defined as $CD11b^{+}CD11c^{-}Gr\text{-}1^{hi}$ cells, monocytes were
141 defined as $CD11b^{+}CD11c^{-}Gr\text{-}1^{med}$ cells, recruited macrophages were defined as
142 $CD11b^{+}CD11c^{-}Gr\text{-}1^{low}$ cells and mast cells were defined as $CD11b^{-}cKit^{+}Fc\varepsilon R1^{+}$ cells. T cells

143 were identified based on gating strategy as described before (Griffiths *et al*., 2016). CD3
144 AF700 (clone 500A2, BD Biosciences), CD4 Pacific blue (clone RM4.5, BD Biosciences),
145 CD44 PeCy7 (clone 1M7, Tonbo Biosciences), CD8 APC Cy7 (clone 53-6.7, BD Biosciences)
146 were used for T-cell surface staining. Fixation/permeabilization concentrate and diluent
147 (eBioscience) were used in the intracellular stain to fix and permeabilize lung cells following
148 manufacturer's instructions. Intracellular staining was performed with IFNγ APC (clone
149 XMG1.2, Tonbo Biosciences) and TNF-α -FITC (Clone MP6-XT22, BD Pharmingen) or the
150 respective isotype control antibodies (APC rat IgG1κ and FITC rat IgG1α isotype, BD
151 Pharmingen) for 30 min. Samples were acquired on a 4 laser BD Fortessa Flow Cytometer and
152 the analysis was performed using FlowJo (Treestar). Total numbers of cells within each gate
153 were back calculated based on cell counts in the individual lung samples.
154
155 **Histological analysis**
156 For mice studies, the left upper lobe was collected for histomorphometric analysis. The lobes
157 were infused with 10% neutral buffered formalin and embedded in paraffin. 5 μm thick ling
158 sections were cut using a microtome, stained with hematoxylin and eosin (H&E) and processed
159 for light microscopy. Images were captured using the automated Nanozoomer digital whole
160 slide imaging system (Hamamatsu Photonics). Regions of inflammatory cell infiltration were
161 delineated utilizing the NDP view2 software (Hamamatsu Photonics), and the percentage of
162 inflammation was calculated by dividing the inflammatory area by the total area of individual
163 lung lobes. All scoring was conducted in a blinded manner.
164 FFPE lung sections from healthy individuals, tuberculosis patients and NHP infected with *MTB*
165 were stained with goat anti-human mast cell chymase (LifeSpan Biosciences, LS-B4134,
166 RRID:AB_10718418) and rabbit anti-human tryptase (Cell Signaling Technology, 195235).
167 Primary antibodies were detected with Alexa fluor 568 donkey anti-goat Ig G (Thermo Fisher

168 Scientific, A-11057, RRID:AB_2534104) and Alexa Fluor 488 donkey anti-rabbit Ig G
169 (Jackson ImmunoResearch Laboratories, 711-546-152, RRID:AB_2340619). Nuclei were
170 labeled with DAPI. MC positive for chymase, tryptase or both were blindly quantitated in 3
171 200x random fields per sample in human and NHP lung sections. 200x pictures were taken
172 with an Axioplan Zeiss microscope and recorded with a Hamamatsu camera.
173
174 **Data analysis and statistics**
175 All data was analyzed using the indicated methodology in each figure legend. Two sided-
176 unpaired t-test was performed for comparing significance between 2 groups, one-way ANOVA
177 Tukey's test and two-way ANOVA Sidak's multiple comparison test were performed for more
178 than 2 groups using GraphPad Prism 5 and 10, respectively (La Jolla, CA). Significance is
179 denoted on the figure and the respective figure legends. Outliers, if any, were removed using
180 Grubb's outlier test and mentioned in the respective figures.
181
182 **Single cell data reanalysis**
183 The NHP single cell lung data was accessed from GEO (GSE149758) and processed through
184 *cellranger 7.0* using the Macaca Mulatta reference genome (Mmul_10). The obtained matrix
185 file was processed through the R package *Seuratv- 5* for downstream analysis of the count
186 matrix. The cells were filtered based on mitochondrial gene content and at least 500 genes
187 detected. Data was log normalized. The most variable genes were detected by the
188 *FindVariableFeatures* function and used for subsequent analysis. Latent variables (number of
189 UMI's and mitochondrial content) were regressed out using a negative binomial model
190 (function *ScaleData*). Principle component analysis (PCA) was performed with the *RunPCA*
191 function. A UMAP dimensionality reduction was performed on the scaled matrix (with most
192 variable genes only) using the first 20 PCA components to obtain a two-dimensional

193 representation of the cell states. For clustering, we used the functions *FindNeighbors* (20 PCA)
194 and *FindClusters* (resolution 0.25). MCs were identified and re-clustered based on expression
195 of the canonical MC marker genes *FCER1A* (High affinity Fc IgE receptor), *CD48*, *FCER1G*
196 (Fc IgE receptor), *MS4A2* (IgE subunit) and *ITGAX* (CD11c) as a negative marker. The cells
197 identified MC cluster (only one cluster) were subset and re-clustered using the method outlined
198 above at a resolution of 0.1. To identify marker genes for mast cells, we used *FindAllMarkers*
199 to compare cluster against all other clusters, and *FindMarkers* to compare selected clusters.
200 For each cluster, only genes that were expressed in more than 15% of cells with at least 0.15-
201 fold differences were considered. The differential genes were subjected to enrichment analysis
202 using Hallmark Pathway gene set from *MsigDB*. The pathways that met an FDR threshold less
203 than 0.05 were considered.
204 Gene signatures were defined with R package *Ucell*. The output is a module signature score
205 generated by *AddModuleScore* function. The obtained score was overlaid on the UMAP and
206 visualized. The Values per cell were extracted and used to plot a summed module U cell score.
207 GraphPad prism was used for the Violin plots and the heatmap. All other figures were
208 generated in R.
209

210 **Results**

211 **Mast cells localize and transition phenotypes within TB granulomas**

212 $MC_T$s were primarily found within the lung from healthy controls (HC), while $MC_C$s or $MC_{TC}$s
213 were found in the lung biopsies of patients with PTB (Garcia-Rodriguez *et al*., 2021). To
214 validate these observations and analyze the compartmentalization of MCs in human lungs, we
215 stained lung biopsies from healthy individuals and patients with PTB to visualize the spatial
216 distribution of $MC_C$s, $MC_T$s and $MC_{TC}$s. Our results show that $MC_C$s are not well represented
217 in the lung parenchyma, interstitium, vasculature, or bronchus of HC lungs (Figure 1A, Figure

218 S1). Instead, we observed that the healthy lungs predominantly contain $MC_T$s and, to a lesser
219 extent, $MC_{TC}$s. While $MC_{TC}$s accumulated in early immature granulomas within TB lesions,
220 $MC_C$s accumulated in late granulomas in TB patients (Figure 1A and B). $MC_T$s also increased
221 in the interstitium, vasculature and bronchus-associated lymphoid tissue of patients with PTB
222 (Figure S1A). Therefore, our study confirmed that $MC_T$s are found in HCs (Garcia-Rodriguez
223 *et al*., 2021) and likely convert first to $MC_{TC}$s in early granulomas before becoming $MC_C$s in
224 late mature granulomas with necrotic cores.
225 Our published data showed that MCs accumulate in the lungs of macaques with PTB compared
226 to LTBI macaque lungs (Esaulova *et al*., 2021). Thus, we next analyzed the accumulation and
227 localization of MCs in the lungs of macaques with LTBI and PTB. We found that similar to
228 human healthy lungs, $MC_T$s accumulated in the lungs of healthy macaques. Although $MC_T$s
229 and these cells increased in some lesions in the lungs of macaques with LTBI, the number of
230 $MC_T$s in macaques with PTB were significantly increased in all sites including granuloma
231 (Figure 1C and D), interstitium as well as vasculature (Figure S1B). Additionally, while $MC_{TC}$s
232 increased in the granulomas of macaques with PTB compared to the lungs of macaques with
233 LTBI and HCs, we did not observe any increase of these cells in other sites within the lung
234 compared to healthy macaques. No $MC_C$s were measurable within macaque lungs. Our data
235 indicate an accumulation of $MC_T$s but not $MC_{TC}$s during LTBI. However, as the disease
236 progresses to PTB, there is an increase in both $MC_{TC}$s and additional $MC_T$s.
237
238 **Lung mast cells express inflammatory and metabolically active transcriptome in**
239 **macaques with PTB**
240 To further understand the transcriptional differences between MCs in lungs of HCs, LTBI and
241 PTB, we re-analyzed the MC subpopulation in the scRNA seq data from macaques from
242 Esauolva *et al*. We examined the single-cell transcriptome of 500 mast cells with unsupervised

243 clustering and identified four clusters, three of which (0,1,3) belonged to PTB group and cluster
244 2 was found exclusively in LTBI and HC (Figure 2A). All the MC clusters were positive for
245 markers such as *FCER1A* (high-affinity IgE receptor), *MS4A2* (IgE subunit), *CD48* (mast cell
246 receptor) and negative for markers like *ITGAX* (macrophage/dendritic cell marker) (Figure 2B).
247 Differential expressed genes (DEGs) among the cluster revealed cluster specific markers.
248 Among the top 10 genes of the largest PTB cluster 0 were *CENPA* (metabolic reprogramming
249 related centromeric protein, (Liang *et al.*, 2021)), *NEK2*, *MELK2* (NF-kB regulator), (Zhang
250 *et al*., 2022)), *CDC20* (role in LC3 mediated autophagy; (Xie *et al*., 2018)), *CDCA5*, *GTSE1*,
251 *CDCA3, ASPM* (proliferation related, (Shen *et al*., 2021), ASPM; (Kouprina *et al*., 2005)), and
252 *BIRC5* (Immunosuppressive and infiltration-associated), genes that were upregulated in MCs
253 from PTB compared to MCs from LTBI and HC lungs. Similarly, the transcriptome of the cells
254 from LTBI and HC expressed high levels of *TUBB6* (inhibitor of pyroptosis, (Salinas *et al*.,
255 2014)), *CD9-1*, *TNFRSF12A* (TNF receptor, needed for anti-TB immunity), *DUSP4,*
256 *HMGCS1*, *LMNA*, *MARCKSL1*, *PHLDA1*, *RGCC* as compared to PTB clusters. The other PTB
257 clusters expressed genes such as *FANCE*, *IL18R1*, *FOS*, *CYTB*, *IL3RA* are genes related to
258 activated mast cells (Figure 2C). Enrichment of cluster specific DEGs revealed enrichment of
259 cholesterol, TNF-α, and TGFβ signaling in LTBI. Oxidative phosphorylation, and IFNγ
260 signaling, and MYC signaling were enriched in the PTB group (Figure 2D). Plotting the
261 summed *Ucell* module scores revealed significant upregulation of IFNγ signaling, Oxidative
262 Phosphorylation and Th2 signature in PTB ($P < 0.05$), while LTBI and HC clusters showed
263 enhanced TNF signaling ($P < 0.05$) (Figure 2E-H). Since we observed increased chymase in
264 MCs of PTB (Figure 1A), we used a chymase signature to compare the PTB with LTBI / HC
265 mast cells. The MCs from PTB (Cluster 0) expressed high levels of chymase, confirming the
266 immunostaining results (Figure 1A). Thus, this analysis provides evidence for the

267 transcriptional heterogeneity in the MCs derived from PTB and LTBI and shows differential
268 activation programs in the cell based on the disease state.
269
270 **MC deficient mice exhibit enhanced control of *Mtb***
271 We next determined if MCs are induced in response to infection in mice following aerosolized
272 low dose *Mtb* infection, and whether they accumulate early or later in infection. Our prior
273 results have shown that innate cells such as ILCs accumulate very early between days 5-10 and
274 followed by accumulation of other innate cells such as neutrophils, macrophages and
275 monocytes between days 10-15 and T cells by day 21 to 30 (Ardain *et al*., 2019). We found
276 that MCs accumulate in the lung at time points between day 21 and 30 and coincide with timing
277 of accumulation of T cells in the lung (data not shown).
278 To further investigate the functional role of MCs in *Mtb* infection, we utilized MC deficient
279 mouse model, *CgKitW*$^{sh}$. Mice carrying spontaneous loss-of-function mutations at both alleles
280 of the dominant *white spotting* (*W*) locus (*i.e.*, c-*kit*) exhibit a marked reduction in c-*kit* tyrosine
281 kinase-dependent signaling resulting in dysregulated mast cell development, survival and
282 function (Wolters *et al*., 2005). We infected *CgKitW*$^{sh}$ mice with low dose aerosolized *Mtb*
283 HN878 and found that compared with wild type control *Mtb*-infected mice, *CgKitW*$^{sh}$ mice did
284 not show any differences in *Mtb* CFU at early time points (50 days post infection (dpi), (Figure
285 3A). However, at later time points (100 dpi and 150 dpi), *CgKitW*$^{sh}$ *Mtb*-infected mice showed
286 significantly lower lung *Mtb* CFU, when compared with *Mtb*-infected wild type control mice
287 (Figure 3B). This coincided with reduced inflammation in the lungs of *CgKitW*$^{sh}$ *Mtb*-infected
288 mice at 150 dpi (Figure 3D and E). Additionally, no differences in *Mtb* CFU were observed at
289 50 dpi in the spleen, *CgKitW*$^{sh}$ *Mtb*-infected mice showed enhanced control of *Mtb* in the spleen
290 at 100 and 150 dpi (Figure 3C). Therefore, *CgKitW*$^{sh}$ mice lacking MCs exhibit better *Mtb*
291 control, specifically during late stages of infection.

292 To mechanistically address the functional basis of enhanced protection, we analyzed the lungs
293 of *CgKitW*$^{sh}$ mice before and after *Mtb* infection as this mouse strain is associated with other
294 known immune deficiencies (Grimbaldeston *et al*., 2005). At baseline, MCs were significantly
295 reduced in the lungs of *CgKitW*$^{sh}$ mice compared to B6 mice. MCs continued to accumulate in
296 the lung up to 100 dpi in *CgKitW*$^{sh}$ mice, following which the MC numbers decreased at later
297 stages. Indeed, the deficiency in MCs observed in lungs of *CgKitW*$^{sh}$ mice was retained
298 following infection until 150 dpi (Figure 4A). However, we also found that at baseline
299 *CgKitW*$^{sh}$ mice also showed increased dendritic cells (DCs) as well as recruited macrophages
300 (RMs) but no perturbations in alveolar macrophages (AMs), neutrophils or monocytes.
301 Additionally, the increased DCs and RMs responses were also evident in *CgKitW*$^{sh}$ mice at 50
302 dpi following infection, but not maintained at later time points (Figure 4B and C). No
303 differences in AMs, neutrophils and monocytes were observed in the lungs of *Mtb*-infected
304 *CgKitW*$^{sh}$ mice when compared with *Mtb*-infected control mice at all time points tested (Figure
305 D, E and F). Previous studies have implicated MCs in driving T cell responses (Elieh *et al*.,
306 2018). At baseline, we found that there is an increase in $CD4^+$ and $CD8^+$ T cells numbers (data
307 not shown), we found no differences in $CD4^+$ and $CD8^+$ T cells responses at 50 dpi, but
308 numbers of activated $CD4^+$ and $CD8^+$ T cells were significantly reduced at 100dpi, which
309 compromised $CD4^+$ IFNγ producing cells as well as TNF-α and IFNγ dual cytokine producing
310 subsets at 100 dpi, in the *CgKitW*$^{sh}$ mice as compared to C57Bl/6 *Mtb*-infected mice (Figure
311 S2). Finally, we measured cytokine responses in the lungs of wild type C57Bl/6 and *CgKitW*$^{sh}$
312 *Mtb*-infected mice at 150 dpi. We found that while proinflammatory cytokines that direct
313 monocyte/macrophage responses and T cell responses including G-CSF, IFNγ, IL-1β, IL-6,
314 IL-17, MCP-1, TNF-α and RANTES were significantly higher in wild type *Mtb*-infected lungs
315 compared with *CgKitW*$^{sh}$ *Mtb* infected lungs, chemokines that direct neutrophil responses such
316 as MIP-1α, MIP-1β, KC and MIP2 and Th2 cytokines like IL-13 were not different between

317 wild type and *CgKitW*$^{sh}$ *Mtb*-infected lungs at 150 dpi (Figure 4G). These results together
318 provide evidence that MCs are induced following *Mtb* infection, accumulate in the lung and
319 mediate cytokine responses to drive pathology and promote *Mtb* susceptibility and
320 dissemination during TB.
321
322 **Discussion**
323 The immune mechanism(s) that mediate the progression from LTBI to PTB are unclear. In this
324 study, we identified MCs as an innate cell type that is overrepresented during PTB,
325 transcriptionally express signatures associated with IFNγ, oxidative phosphorylation, and
326 MYC signaling, and localize within mature TB granulomas. Importantly, using mice deficient
327 in MCs, we show a potential pathological role for MCs in mediating susceptibility to TB.
328 Together, this paper provides evidence of MCs in the context of pathology and susceptibility
329 to TB providing MCs as a novel therapeutic platform.
330 MCs have been shown to interact with *Mtb* through the GPI anchored molecule CD48 (Munoz
331 *et al*., 2003), interaction with TLR2 (Carlos *et al*., 2007) and potentially TLR4 (McCurdy, Lin,
332 & Marshall, 2001). Additionally, *Mtb* is also thought to be internalized by lipid rafts on MCs
333 (Munoz *et al*., 2009), thus serving as a long lasting reservoir for *Mtb* (da Silva *et al.,* 2014). In
334 in vitro studies, MC exposure to *Mtb* resulted in degranulation of MCs as well as induction of
335 proinflammatory cytokines such as TNF-α and IL-1β. While these studies using high dose
336 model of infection reported early induction of inflammatory mediators from MC within hours
337 to days, our in vivo results using a physiological low dose of *Mtb* infection model show that
338 MCs accumulate between 21-30 days coinciding with accumulation of T cells in the lung.
339 Interestingly, despite accumulation of MCs in the lung at 30 dpi following low dose aerosol
340 infection, the impact of MC deficiency on *Mtb* control and inflammation in *CgKitW*$^{sh}$ mice is
341 not evident until 100 dpi. This is similar to our published studies where we found that S100A8/9

342 deficiency resulted in reduced neutrophil lung accumulation (Scott *et al*., 2020), resulted in
343 improved *Mtb* control and improved TB disease, but after 100 dpi. This is in contrast to the
344 role of eosinophils in TB, where eosinophil deficiency resulted in increased *Mtb* CFU (Bohrer
345 *et al*., 2021). MCs are the primary cell type defective in the lungs of *CgKitW*$^{sh}$ mice at baseline
346 and at all time points following infection, thus, we attribute the improved *Mtb* control with MC
347 deficiency. However, we do report increased RMs and DCs accumulation at baseline in
348 *CgKitW*$^{sh}$ mice, but these changes are not maintained until 100 dpi, a time point when we see
349 impact on *Mtb* control. Additionally, the reduced inflammation observed at 100 and 150 dpi is
350 associated with decreased level of proinflammatory cytokines and chemokines that recruit
351 monocytes/macrophages and T cells, but not chemokines that are associated with neutrophil
352 recruitment. These results imply an important role for MCs in amplifying
353 macrophage/monocyte accumulation during chronic TB and driving increased lung pathology.
354 Overall, based on our results along with the current literature, we propose pathological roles
355 for neutrophils and MCs, while other granulocytes such as eosinophils may mediate protective
356 roles (Bohrer *et al*., 2021).
357 MCs can release cytokines and chemokines, antimicrobial peptides and granules upon
358 pathogen sensing and to control pathogens (Naqvi *et al.,* 2020). In the context of *Mtb* exposure,
359 MCs have been shown to undergo degranulation including histamine and β-hexosaminidase
360 (Munoz *et al*., 2003). Indeed, histamine deficient mice showed decreased neutrophils, as well
361 as proinflammatory cytokine production following *Mtb* infection (Carlos *et al*., 2009).
362 Additionally, induction of degranulation following intratracheal *Mtb* infection resulted in
363 reduced proinflammatory cytokines as well as reduced lung inflammation. With respect to
364 *CgKitW*$^{sh}$ *Mtb*-infected mice, except lower numbers of DCs and $CD4^+$ and $CD8^+$ T cell
365 responses at 100 dpi, we did not find any significant differences in accumulation of innate or
366 adaptive myeloid populations in the lung at other time points. Incidentally decreased numbers

367 of DCs and T cells at 100 dpi was reflected with reduced lung inflammation at 100 dpi. Thus,
368 together with published work, while MCs can potentially modulate neutrophil and other
369 inflammatory mediators in high dose models, in a physiologically relevant *Mtb* infection
370 model, absence of MCs impacted late TB disease and improved *Mtb* control without significant
371 changes to other innate cells. The exact mechanism by which MCs contributing to pathology,
372 dissemination and promoting *Mtb* is an area of future investigation.
373 At baseline, human lungs have been reported to primarily express tryptase (Poto *et al*., 2022)
374 Indeed, we found that this is true for both macaque and human lungs in our study where healthy
375 lungs expressed $MC_{T}$s. Additionally, we found that early granulomas and in LTBI we saw
376 expression of $MC_{TC}$s with a switch to more and accumulation of $MC_{C}$s in late stage
377 granulomas. Chymase expression may modulate extracellular matrix components (ECM) such
378 as fibronectin leading to tissue remodeling, impacting cellular communication and inducing
379 cleavage for key cytokine such as IL-6, IL-13, IL-15, and IL-33, as well as Transforming
380 Growth Factor (TGF-β) (Pejler, 2020; Waern *et al*., 2013). Studies have shown that tryptase
381 can induce proliferation of fibroblasts, epithelial cells and smooth muscle cells, causing airway
382 remodeling during diseased conditions (Mogren *et al*., 2021). Tryptase can also inactivate a
383 large range of peptides by cleaving specific substrates, such as fibrinogen, gelatin, pro-matrix
384 metalloproteinases (MMP) and complement factors thus moderating inflammatory responses
385 (Caughey, 2007). Based on our results from human and macaque lung, we hypothesize that
386 $MC_{TC}$s may synergize to drive responses induced by both pathways at early time points and
387 possibly just by $MC_{C}$s at later time points. Additional studies describing these subsets and
388 testing their functional relevance in *in vivo* models are future steps in delineating the role of
389 these subsets in TB.
390 Analysis of the single cell transcriptome from lungs of macaques identified that the MCs from
391 PTB animals show closer resemblance to $MC_{CS}$ with higher IFNγ, metabolic activation and

392 expression of *CMTA* gene and chymase signature, although all the MCs (from PTB, LTBI and
393 HC) had a minimal tryptase signature. MCs are known to gear towards a Th2 signature with
394 increased chymase expression (Toru *et al*., 1998). This increase was reflected in MCs from the
395 macaque lung, showing a high transcriptomic Th2 signature in PTB but not in clusters found
396 in LTBI and HC. In essence transcriptomics reflected the hyperactivated nature of the MCs in
397 PTB, which might make them more pathologic during infection. Although our *in vivo* mouse
398 study shows pathological role of MCs, significant secretion of Th2 cytokines are not seen,
399 likely because the C57Bl/6 mouse model is prone towards Th1 polarization (Wakeham, *et al*.,
400 2000). MCs have the ability to release both preformed and de novo synthesized TNF-α, hence
401 helping in early bacterial clearance (Gordon and Galli, 1991). Similarly, our study shows that
402 the MCs from HC and LTBI individuals expressed higher levels of TNF-α, and in less-
403 metabolically activated state (lower OXPHOS signature). So additional studies will help in
404 elucidating the mechanism through which MCs mediate pathological roles.
405 In summary, we demonstrate that accumulation of chymase producing MC in PTB is a cross-
406 species phenomenon that contributes to increased TB pathology and loss of TB control, thereby
407 elucidating the pathological role of MCs in the control of *Mtb* infection. By targeting MC
408 pathways or signaling mechanisms, host-directed therapies (HDTs) hold the promise of
409 enhancing the effectiveness of existing treatments and mitigating disease-related
410 complications.
411
412
413
414
415
416

**Acknowledgements**

This work was supported by Washington University in St. Louis; NIH grant HL105427, AI111914, AI134236 and AI123780 to S.A.K., and the Department of Microbiology, University of Chicago. We thank Ms. Lan Lu, Washington University in St. Louis and Ms. Tao Yun, University of Chicago for technical support and assistance.

**Authors Contributions**

S.A.K supervised all aspects of the study. A.G. designed, performed experiments, and analyzed data. A.G., V.T., A.A., and K.S.C. curated data and constructed figures. V.T, J.R.M, M.A., N.N. and K.S.C. contributed resources and/or data analysis. A.G. and S.A.K wrote the original draft of the manuscript. A.G., A.A., N.N., V.T., and S.A.K. reviewed and edited the manuscript. J.Z. provided human specimen. D.K. provided NHP specimen, D.K and S.A.K provided funding. All authors reviewed, edited and approved the manuscript.

**Competing interests.**

The authors declare no competing interests.

434 **References**


435 Ardain A, Domingo-Gonzalez R, Das S, Kazer S W, Howard NC, Singh A, Khader SA.
436 2019. Group 3 innate lymphoid cells mediate early protective immunity against tuberculosis.
437 *Nature* **570**: 528-532. DOI: https://doi.org/10.1038/s41586-019-1276-2, PMID: 31168092

438 Bian G, Gu Y, Xu C, Yang W, Pan X, Chen Y, Ma F. 2021. Early development and
439 functional properties of tryptase/chymase double-positive mast cells from human pluripotent
440 stem cells. *Journal of Molecular Cell Biology* **13**: 104-115. DOI:
441 https://doi.org/10.1093/jmcb/mjaa059, PMID: 33125075
442

443 Bohrer AC, Castro E, Hu Z, Queiroz ATL, Tocheny CE, Assmann M, Mayer-Barbe KD.
444 2021. Eosinophils are part of the granulocyte response in tuberculosis and promote host
445 resistance in mice. *Journal of Experimental Medicine* **218**. DOI:
446 https://doi.org/10.1084/jem.20210469, PMID: 34347010

447 Carlos D, de Souza Junior DA, de Paula L, Jamur MC, Oliver C, Ramos SG, Faccioli LH.
448 2007. Mast cells modulate pulmonary acute inflammation and host defense in a murine
449 model of tuberculosis. *Journal of Infectious Diseases* **196**: 1361-1368. DOI:
450 https://doi.org/10.1086/521830, PMID: 34347010

451 Carlos D, Fremond C, Samarina A, Vasseur V, Maillet I, Ramos SG, Ryffel B. 2009.
452 Histamine plays an essential regulatory role in lung inflammation and protective immunity in
453 the acute phase of Mycobacterium tuberculosis infection. *Infection and Immunity* **77**: 5359-
454 5368. DOI: https://doi.org/10.1128/IAI.01497-08, PMID: 19822651

455 Caughey GH. 2007. Mast cell tryptases and chymases in inflammation and host defense.
456 *Immunological Reviews* **217**: 141-154. DOI: https://doi.org/10.1111/j.1600
457 065X.2007.00509.x, PMID: 17498057

458 da Silva EZ, Jamur MC,Oliver C. 2014. Mast cell function: a new vision of an old cell.
459 *Journal of Histochemistry Cytochemistry* **62**:698-738. DOI:
460 https://doi.org/10.1369/0022155414545334, PMID: 25062998

461 Esaulova E, Das S, Singh DK, Choreno-Parra JA, Swain A, Arthur L, Khader, SA. 2021. The
462 immune landscape in tuberculosis reveals populations linked to disease and latency. *Cell*
463 *Host and Microbe* **29**: 165-178 e168. DOI: https://doi.org/10.1016/j.chom.2020.11.013,
464 PMID: 33340449

465 Elieh AKD, Grauwet K. 2018. Role of Mast Cells in Regulation of T Cell Responses in
466 Experimental and Clinical Settings. *Clinical Reviews in Allergy and Immunology* **54**: 432-
467 445.DOI: https://doi.org/10.1007/s12016-017-8646-z, PMID: PMID: 28929455

468 Garcia-Rodriguez KM, Bini EI, Gamboa-Dominguez A, Espitia-Pinzon CI, Huerta-Yepez S,
469 Bulfone-Paus S, Hernandez-Pando R. 2021. Differential mast cell numbers and
470 characteristics in human tuberculosis pulmonary lesions. *Scientific Reports* **11**: 10687. DOI:
471 https://doi.org/10.1038/s41598-021-89659-6, PMID: 34021178

472 Gopal R, Rangel-Moreno J, Slight S, Lin Y, Nawar HF, Fallert Junecko BA, Khader, SA.
473 2013. Interleukin-17-dependent CXCL13 mediates mucosal vaccine-induced immunity
474 against tuberculosis. *Mucosal Immunology* **6**: 972-984. DOI:
475 https://doi.org/10.1038/mi.2012.135, PMID: 23299616

476• Griffiths, K., Ahmed, M., Das, S., Gopal, R., Horne, W., Connell, TD., Moynihan, KD.,
477 Kolls, JK., Irvine, DJ., Artyomov, MN., Rangel-Moreno, J., Khader, SA. 2016. Targeting
478 dendritic cells to accelerate T-cell activation overcomes a bottleneck in tuberculosis vaccine
479 efficacy. *Nature Communications* **7**: 13894. DOI: https://doi.org/10.1038/ncomms13894,
480 PMID: 28004802

481 Grimbaldeston MA, Chen CC, Piliponsky AM, Tsai M, Tam SY, Galli SJ. 2005. Mast cell-
482 deficient W-sash c-kit mutant Kit W-sh/W-sh mice as a model for investigating mast cell
483 biology in vivo. *The American Journal of Pathology* **167**: 835-848.DOI:
484 https://doi.org/10.1016/S0002-9440(10)62055-X, PMID: 16127161

485 Gordon J R, Galli S J. 1991. Release of both preformed and newly synthesized tumor
486 necrosis factor alpha (TNF-alpha)/cachectin by mouse mast cells stimulated via the Fc
487 epsilon RI. A mechanism for the sustained action of mast cell-derived TNF-alpha during IgE-
488 dependent biological responses. *Journal of Experimental Medicine* **174**: 103-107. DOI:
489 https://doi.org/10.1084/jem.174.1.103, PMID: 1829107

490 Khader SA, Bell GK, Pearl JE, Fountain JJ, Rangel-Moreno J, Cilley GE, Cooper AM. 2007.
491 IL-23 and IL-17 in the establishment of protective pulmonary CD4+ T cell responses after
492 vaccination and during Mycobacterium tuberculosis challenge. *Nature Immunolog,* **8**:369-
493 377. DOI: https://doi.org/10.1038/ni1449, PMID: 17351619

494 Kouprina N, Pavlicek A, Collins NK, Nakano M, Noskov VN, Ohzeki J, Larionov V. 2005.
495 The microcephaly ASPM gene is expressed in proliferating tissues and encodes for a mitotic
496 spindle protein. *Human Molecular Genetics* **14**:2155-2165. DOI:
497 https://doi.org/10.1093/hmg/ddi220, PMID: 15972725

498 Liang YC, Su Q, Liu YJ, Xiao H,Yin HZ. 2021. Centromere Protein A (CENPA) Regulates
499 Metabolic Reprogramming in the Colon Cancer Cells by Transcriptionally Activating
500 Karyopherin Subunit Alpha 2 (KPNA2). *American Journal of Pathology* **191**:2117-2132.
501 DOI: https://doi.org/10.1016/j.ajpath.2021.08.010, PMID: 34508688

502 McCurdy JD, Lin TJ, Marshall, JS. 2001. Toll-like receptor 4-mediated activation of murine
503 mast cells. *Journal of Leukocyte Biology* **70**: 977-984. PMID: 11739561

504 Mogren S, Berlin F, Ramu S, Sverrild A, Porsbjerg C, Uller L, Andersson CK. 2021. Mast
505 cell tryptase enhances wound healing by promoting migration in human bronchial epithelial
506 cells. *Cell Adhesion and Migration* **15**, 202-214. DOI: https://doi.org/
507 10.1080/19336918.2021.1950594, PMID: 34308764

508 Munoz S, Hernandez-Pando R, Abraham SN, Enciso JA. 2003. Mast cell activation by
509 Mycobacterium tuberculosis: mediator release and role of CD48. *Journal of Immunology*
510 **170:**5590-5596. DOI: https://doi.org/10.4049/jimmunol.170.11.5590, PMID: 12759438

511 Munoz S, Rivas-Santiago B, Enciso JA. 2009. Mycobacterium tuberculosis entry into mast
512 cells through cholesterol-rich membrane microdomains. *Scandavian Journal of Immunology*
513 **70**:256-263. DOI: https://doi.org/10.1111/j.1365-3083.2009.02295.x, PMID: 19703015

514 Naqvi N, Srivastava R, Naskar P, Puri N. 2021. Mast cells modulate early responses to
515 Mycobacterium bovis Bacillus Calmette-Guerin by phagocytosis and formation of
516 extracellular traps. *Cellular Immunology* **365**: 104380. DOI:
517 https://doi.org/10.1016/j.cellimm.2021.104380, PMID: 34049012

518 Naqvi N, Srivastava R, Selvapandiyan A, Puri N. 2020. Host Mast Cells in Leishmaniasis:
519 Friend or Foe? *Trends of Parasitology* **36**: 952-956. DOI:
520 https://doi.org/10.1016/j.pt.2020.09.010, PMID: 33060062

521 World Health Organization, 2023. Global Tuberculosis Report Retrieved from
522 https://www.who.int/teams/global-tuberculosis-programme/tb-reports/global-tuberculosis-
523 report-2023.

524 Pejler G. 2020. Novel Insight into the in vivo Function of Mast Cell Chymase: Lessons from
525 Knockouts and Inhibitors. *Journal of Innate Immunology* **12**: 357-372. DOI:
526 https://doi.org/10.1159/000506985, PMID: 32498069

527 Poto R, Criscuolo G, Marone G, Brightling CE, Varricchi G.2022. Human Lung Mast Cells:
528 Therapeutic Implications in Asthma. *International Journal of Molecular Sciences* **23**. DOI:
529 https://doi.org/10.3390/ijms232214466, PMID: 36430941

530 Salinas RE, Ogohara C, Thomas MI, Shukla KP, Miller SI, Ko DC. 2014. A cellular genome
531 wide association study reveals human variation in microtubule stability and a role in
532 inflammatory cell death. *Molecular Biology of the Cell* **25**:76-86. DOI:
533 https://doi.org/10.1091/mbc.E13-06-0294, PMID: 24173717

534 Scott NR, Swanson RV, Al-Hammadi N, Domingo-Gonzalez R, Rangel-Moreno J, Kriel BA,
535 Khader SA. 2020. S100A8/A9 regulates CD11b expression and neutrophil recruitment during
536 chronic tuberculosis. *Journal of Clinical Investigation,* **130**: 3098-3112. DOI:
537 https://doi.org/10.1172/JCI130546, PMID: 32134742

538 Shen D, Fang Y, Zhou F, Deng Z, Qian K, Wang G, Wang X. 2021. The inhibitory effect of
539 silencing CDCA3 on migration and proliferation in bladder urothelial carcinoma. *Cancer*

540 *Cell International* **21**: 257. DOI: https://doi.org/10.1186/s12935-021-01969-x,
541 PMID: 33980246

542 Toru H, Eguchi M, Matsumoto R, Yanagida M, Yata J, Nakahata T. 1998. Interleukin-4
543 promotes the development of tryptase and chymase double-positive human mast cells
544 accompanied by cell maturation. *Blood,* **91**:187-195. PMID: 9414284

545 Waern I, Lundequist A, Pejler G, Wernersson S. 2013. Mast cell chymase modulates IL-33
546 levels and controls allergic sensitization in dust-mite induced airway inflammation. *Mucosal*
547 *Immunol* **6**: 911-920. DOI: https://doi.org/10.1038/mi.2012.129, PMID: 23235745

548 Wakeham J, Wang J, Xing Z. 2000. Genetically determined disparate innate and adaptive
549 cell-mediated immune responses to pulmonary Mycobacterium bovis BCG infection in
550 C57BL/6 and BALB/c mice. *Infection and Immunity,* **68**:6946-6953. DOI:
551 https://doi.org/10.1128/IAI.68.12.6946-6953.2000, PMID: 11083818

552 Wolters PJ, Mallen-St Clair J, Lewis CC, Villalta SA, Baluk P, Erle DJ, Caughey GH. 2005.
553 Tissue-selective mast cell reconstitution and differential lung gene expression in mast cell-
554 deficient $Kit^{(W\text{-}sh)}/Kit^{(W\text{-}sh)}$ sash mice. *Clinical and Experimental Allergy, **35***: 82-88. DOI:
555 https://doi.org/10.1111/j.1365-2222.2005.02136.x, PMID: 15649271

556 Xie YP, Lai S, Lin QY, Xie X., Liao JW, Wang HX, Li HH. 2018. CDC20 regulates cardiac
557 hypertrophy via targeting LC3-dependent autophagy. *Theranostics* **8:** 5995-6007. DOI:
558 https://doi.org/10.7150/thno.27706, PMID: 30613277

559 Zhang Y, Lu R, Huang X, Yin E, Yang Y, Yi C, Yuan, X. 2022. Circular RNA MELK
560 Promotes Chondrocyte Apoptosis and Inhibits Autophagy in Osteoarthritis by Regulating

561 MYD88/NF-kappaB Signaling Axis through MicroRNA-497-5p. *Contrast Media Molecular*
562 *Imaging* **2022**: 7614497. DOI: https://doi.org/10.1155/2022/7614497, PMID: 35992546
563
564
565

566 **Figure legends**

567 **Figure 1. Chymase positive mast cells are predominant in TB infected human and**
568 **macaque lung tissue.** Lung biopsies from healthy individuals (n = 4) or patients with PTB (n
569 = 5) were stained for tryptase $MC_T$ (green) or chymase $MC_C$ (red). (A) Immunofluorescence
570 microscopy shows $MC_{TS}$ (green) in healthy lung biopsies (HC). $MC_{TCS}$ (red and green merge)
571 are located around the early granulomas, while $MC_{CS}$ (red) surround the late granulomas in TB
572 infected lung biopsies. (B) Predominance of $MC_{TS}$ in healthy lungs transitioning to $MC_{TCS}$ in
573 early granuloma and becoming $MC_{CS}$ in late granulomas in TB infected lungs. (C)
574 Immunofluorescence microscopy shows $MC_{TS}$ (green) and $MC_{TCS}$ (merge) in lungs of healthy
575 (HC), LTBI and PTB macaques. (D) Predominance of $MC_{TS}$ (green) and $MC_{TCS}$ (merge) in
576 PTB compared to LTBI and HC. Statistical analysis was performed using unpaired, 2-tailed
577 Student's t test, **** $p < 0.0001$, *** $p < 0.001$, * $p< 0.05$.

578

579 **Figure 2. Mast cells in lung in active TB show an inflammatory and metabolically active**
580 **transcriptome as compared to HC or LTBI.** Single-cell (sc) RNA-seq Data was re-analyzed
581 from the lung of non-human primates (Esauolva *et al*). (A) UMAP embedding of the *FCER1A*$^+$
582 mast cells, revealed four transcriptionally distinct clusters; the distribution of the MCs across
583 disease condition is indicated by the color PTB (pink), HC (green) and LTBI (blue). (B)
584 Showing the average expression of MCs specific marker genes (*FCER1A*, *MS4A2* and *CD48*)
585 and a macrophage gene *ITGAX* in contrast. (C) Dot plot indicating expression of top
586 differentially expressed genes detected for each cell cluster identified. The dot color represents
587 the expression level, and the dot size represents the percentage of cells in each cluster
588 expressing a particular gene. (D) Hallmark Pathway analysis of the differential genes, only top
589 pathways with highest FDR in each cluster is plotted. The color indicates the –log10 FDR; E-
590 H) UMAP plots with the U cell module score (averaged score of all genes) of the pathways

591 and their corresponding violin plots. Cluster 2 from LTBI/HC were compared to the rest of the
592 PTB groups using a Kruskal-Wallis test with Dunn's multiple correction. **** $p < 0.0001$, ***
593 $p < 0.001$, ns: not significant.
594
595 **Figure 3: MC deficient mice are resistant to *Mtb* chronic infection.**
596 (A) C57BL/6 and CgKitW$^{sh}$ mice were infected with a low aerosol dose (~100CFU) of *Mtb*
597 HN878 and mice were sacrificed at 50, 100 and 150 dpi. (B) Bacterial burden was assessed in
598 lungs and spleens by plating. (C) Lungs were harvested, fixed in formalin and embedded in
599 paraffin. H&E staining was caried out for blinded and unbiased analysis of histopathology. (D)
600 Representative images and the area of inflammation measured in each lobe is shown. Scale
601 bars: 2mm. Original magnification: ×20. Data points represent the mean ± SD of two
602 experiments ($n$ = 8-15 per time point per group). Statistical analysis was performed using
603 unpaired, 2-tailed Student's t test between C57BL/6 and *CgKitW$^{sh}$* mice, **** $p < 0.0001$, ***
604 $p < 0.001$, * $p < 0.05$.
605
606 **Figure 4: MC deficient mice have dysregulated immune profile after *Mtb* infection.**
607 C57BL/6 and *CgKitW$^{sh}$* mice were infected with a low aerosol dose (~100CFU) of *Mtb* HN878
608 and mice were sacrificed at 50, 100 and 150 dpi. Number of (A) mast cells, (B) dendritic cells,
609 (C) recruited macrophages, (D) alveolar macrophages, (E) neutrophils and (F) monocytes were
610 enumerated in the lungs of *Mtb* infected mice. (G) Cytokine and chemokines production in
611 lung homogenates from mice, collected at 150dpi, was assessed by multiplex cytokine analysis.
612 Data points represent the mean ± SD of 1 of 2 individual experiments ($n$ = 5-8 per time point
613 per group). Statistical analysis was performed using unpaired, 2-tailed Student's t test for (A)
614 to (F) and Two-way ANOVA Sidak's multiple comparison test for (G) between C57BL/6 and

615 *CgKitW*$^{sh}$ mice, *** $p < 0.0001$, ** $p < 0.001$, * $p < 0.05$. Outliers were removed from the

616 subsets using Grubb's outlier test.

617

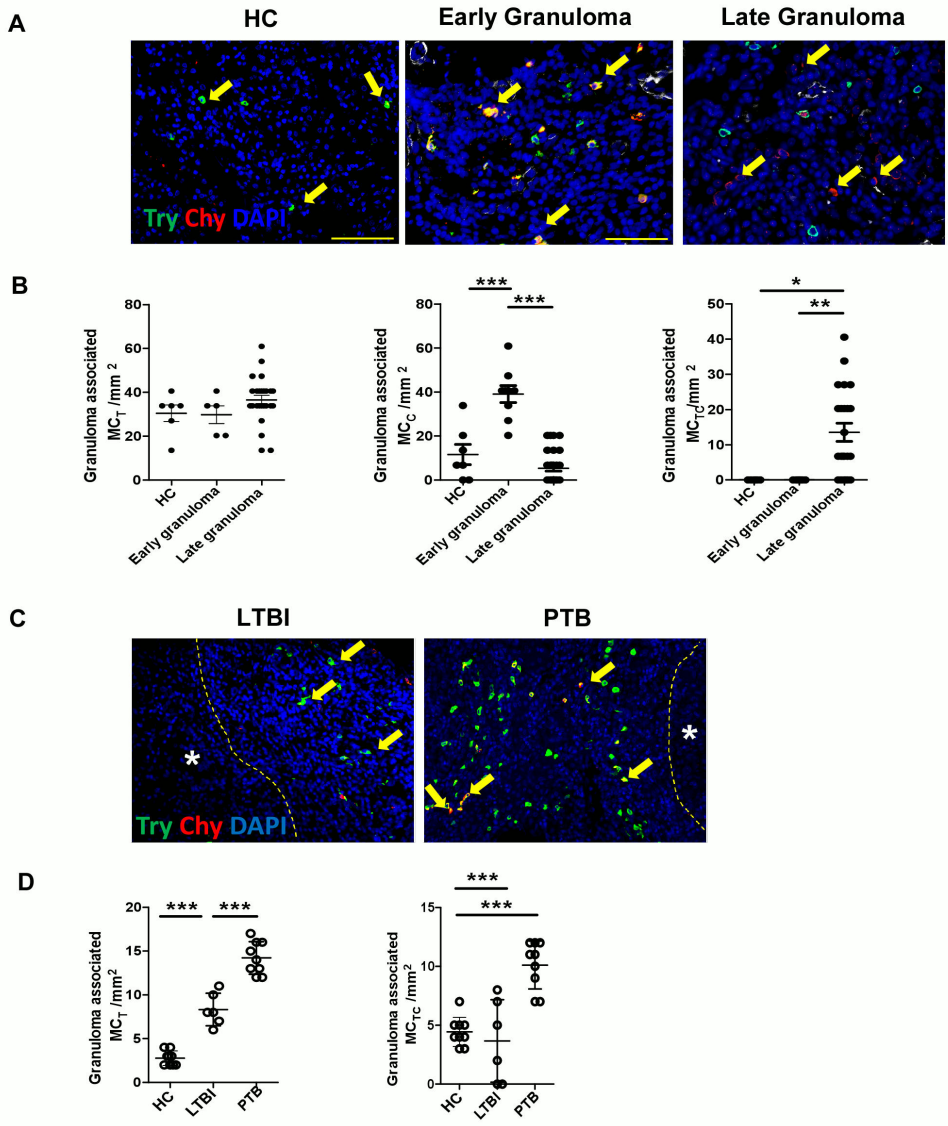
A
HC
Early Granuloma
Late Granuloma
Try Chy DAPI
B
Granuloma associated MC$_T$ /mm$^2$
Granuloma associated MC$_C$ /mm$^2$
Granuloma associated MC$_{TC}$ /mm$^2$
HC
Early granuloma
Late granuloma
***
*
**
C
LTBI
PTB
Try Chy DAPI
D
Granuloma associated MC$_T$ /mm$^2$
Granuloma associated MC$_{TC}$ /mm$^2$
HC
LTBI
PTB
***

**Figure 1**

618

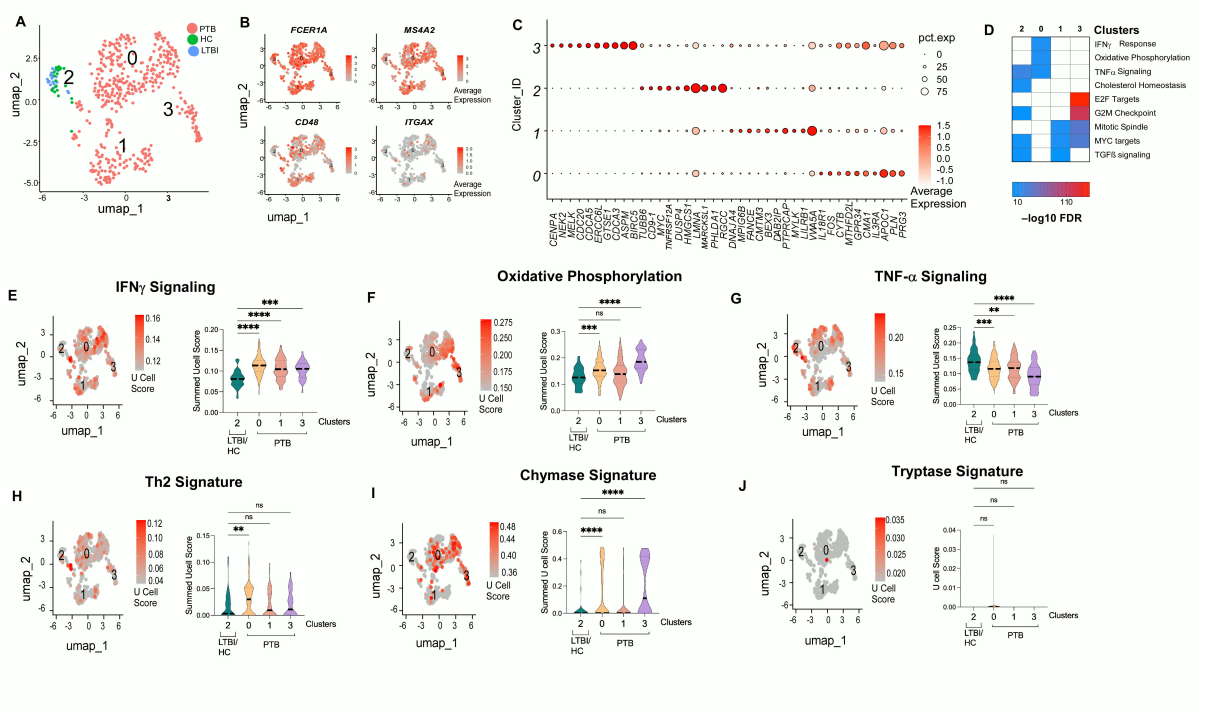
A
PTB
HC
LTBI
umap_2
umap_1
B
FCER1A
MS4A2
CD48
ITGAX
Average Expression
C
Cluster_ID
pct.exp
Average Expression
D
Clusters
IFNγ Response
Oxidative Phosphorylation
TNFα Signaling
Cholesterol Homeostasis
E2F Targets
G2M Checkpoint
Mitotic Spindle
MYC targets
TGFß signaling
−log10 FDR
E
IFNγ Signaling
F
Oxidative Phosphorylation
G
TNF-α Signaling
H
Th2 Signature
I
Chymase Signature
J
Tryptase Signature
U Cell Score
Summed Ucell Score
Clusters
LTBI/ HC
PTB

**Figure 2**

619

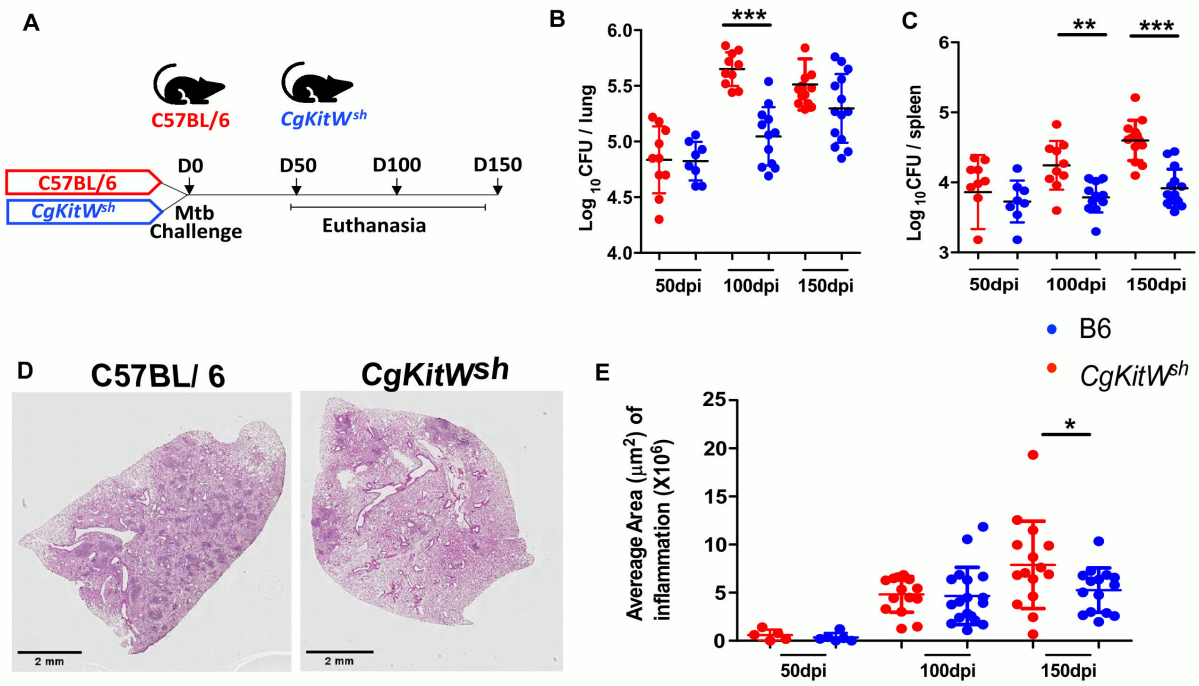
A
C57BL/6
CgKitWsh
C57BL/6
CgKitWsh
D0
D50
D100
D150
Mtb
Challenge
Euthanasia
B
Log 10 CFU / lung
6.0
5.5
5.0
4.5
4.0
***
50dpi
100dpi
150dpi
C
Log 10 CFU / spleen
6
5
4
3
**
***
50dpi
100dpi
150dpi
B6
CgKitWsh
D
C57BL/ 6
CgKitWsh
2 mm
2 mm
E
Avereage Area (µm2) of inflammation (X106)
25
20
15
10
5
0
*
50dpi
100dpi
150dpi

**Figure 3**

620

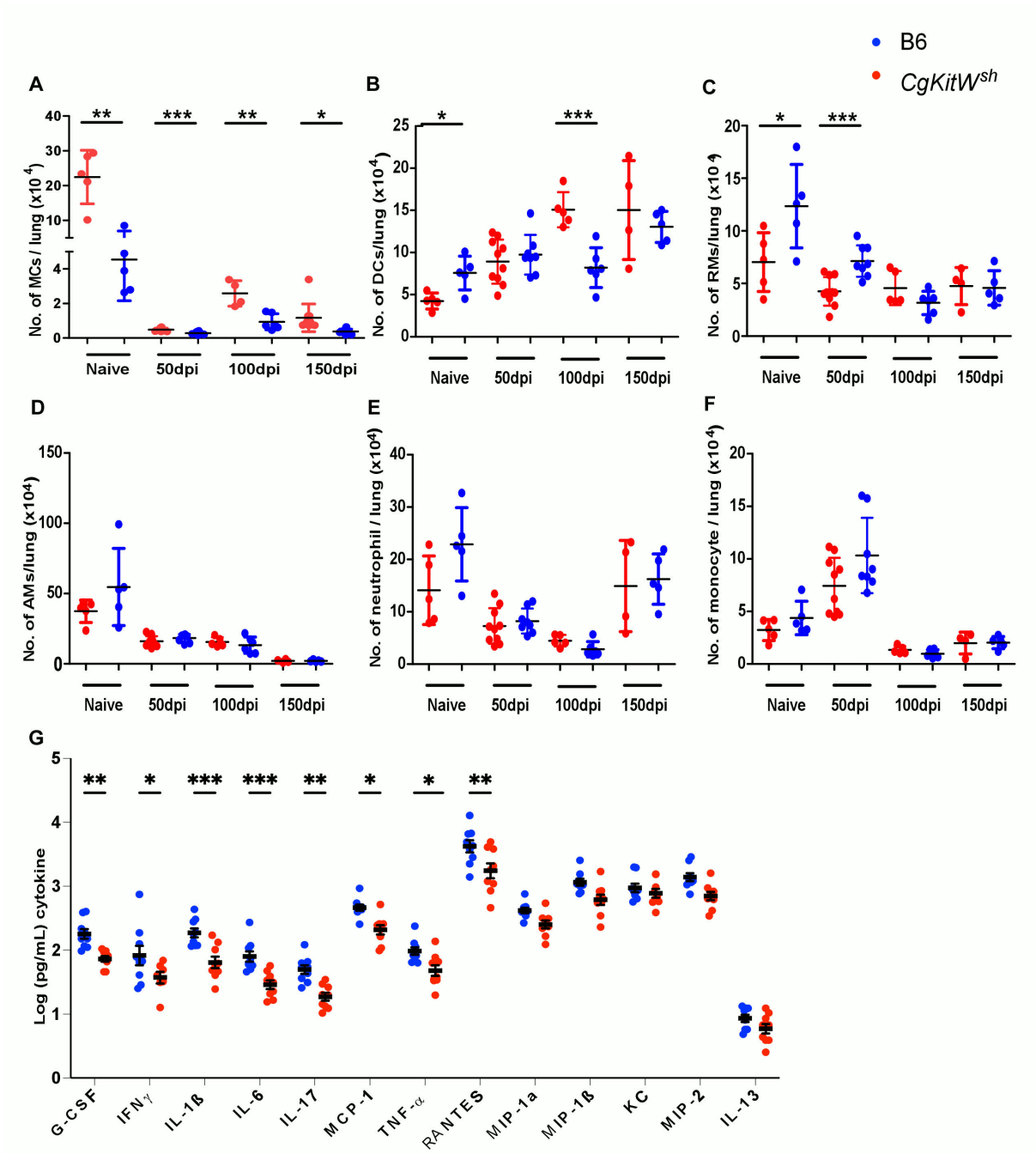


**Figure 4**

621

622

623

624

625

626 **Figure S1: Predominance of $MC_T$s in human and NHPs lung interstitium, blood vessels**
627 **and bronchi.**
628 Healthy lung tissue and TB infected biopsies from human and NHP samples were stained for
629 $MC_T$ (green), $MC_C$ (red). Accumulation and localization of (A) $MC_{TS}$, (B) $MC_{CS,}$ and (C)
630 $MC_{TCS}$ in healthy and TB infected human lung, and (D) $MC_{TS}$ and (E) $MC_{TCS}$ in LTBI and TB
631 macaque lungs. Statistical analysis was performed using unpaired, 2-tailed Student's t test, ***
632 $p < 0.0001$, ** $p < 0.001$, * $p< 0.05$.
633
634 **Figure S2: MC deficient mice have reduced numbers of activated $CD4^+$ and $CD8^+$ T cells**
635 **in lung.** C57BL/6 and $CgKitW^{sh}$ mice were infected with a low aerosol dose (~100CFU) of
636 *Mtb* HN878 and mice were sacrificed at 50, 100 and 150 dpi. Number of (A) $CD4^+$ $CD44^+$T
637 cells, (B) $CD4^+$ $CD44^+$ $IFN\gamma^+$ T cells, (C) $CD4^+$ $CD44^+$TNF-$\alpha^+$ T cells (D) $CD4^+$ $CD44^+$ $IFN\gamma^+$
638 TNF-$\alpha^+$ T cells, (E) $CD8^+$ $CD44^+$T cells, (F) $CD8^+$ $CD44^+$ $IFN\gamma^+$ T cells, (G) $CD8^+$ $CD44^+$
639 TNF-$\alpha^+$ T cells, and (H) $CD8^+$ $CD44^+$ $IFN\gamma^+$ TNF-$\alpha^+$ T cells in the lungs of *Mtb* infected mice.
640 Data points represent the mean ± SD of 1 of 2 individual experiments ($n$ = 5-8 per time point
641 per group). Statistical analysis was performed using unpaired, 2-tailed Student's t test between
642 C57BL/6 and $CgKitW^{sh}$ mice, *** $p < 0.0001$, ** $p < 0.001$, * $p< 0.05$. Outliers were removed
643 from the subsets using Grubb's outlier test.

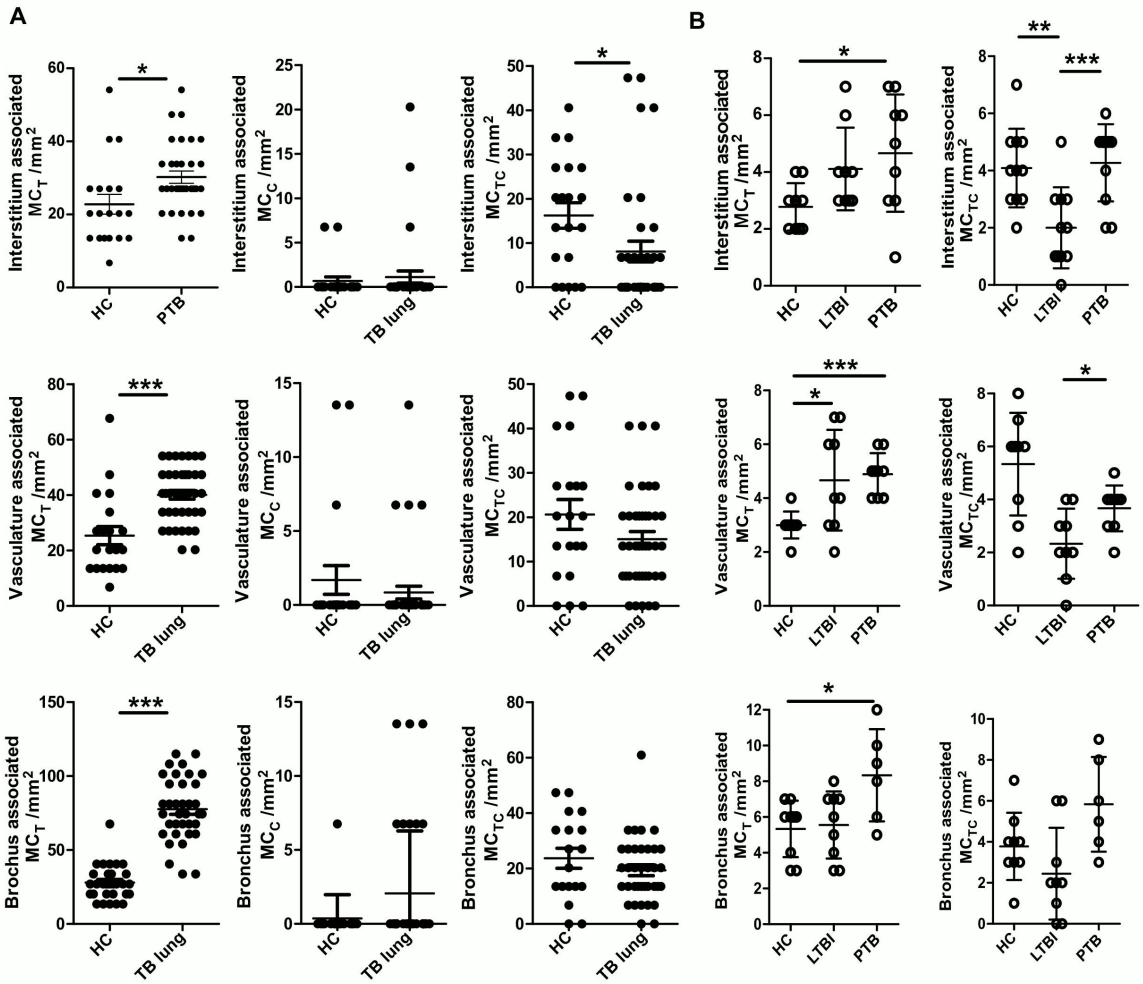


**Figure S1**

644

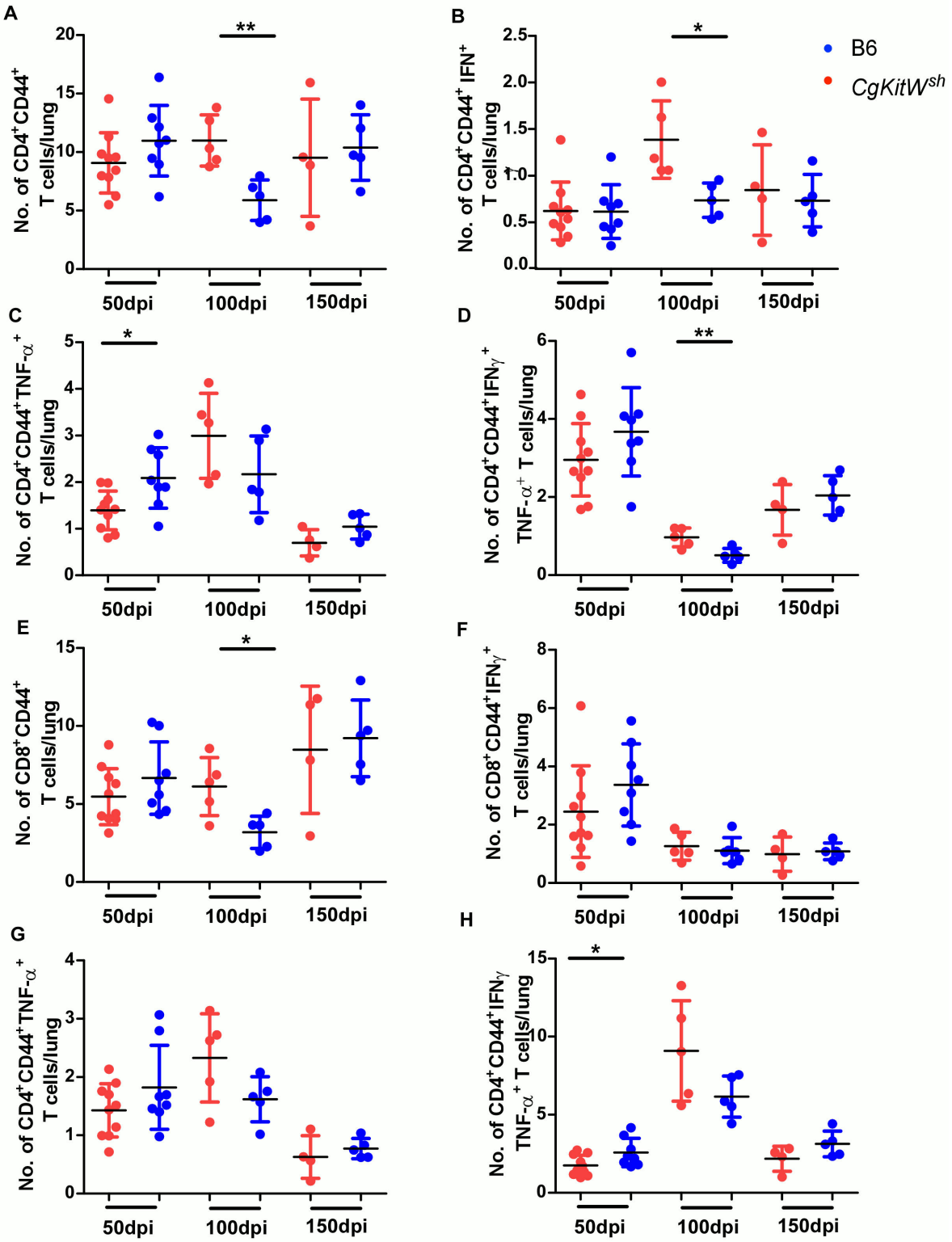


**Figure S2**

645